Wannier-based implementation of the coherent potential approximation with applications to Fe-based transition metal alloys

Naohiro Ito [1],[*] Takuya Nomoto,[2] Koji Kobayashi [3] Sergiy Mankovsky [4] Kentaro Nomura,[3,5]
Ryotaro Arita [2,6] Hubert Ebert [4] and Takashi Koretsune[1]

[1]*Department of Physics, Tohoku University, Sendai 980-8578, Japan*
[2]*Department of Applied Physics, The University of Tokyo, Hongo, Bunkyo-ku, Tokyo 113-8656, Japan*
[3]*Institute for Materials Research, Tohoku University, Sendai 980-8577, Japan*
[4]*Department Chemie, Physikalische Chemie, Universität München, Butenandstrasse 5-13, 81377 München, Germany*
[5]*Center for Spintronics Research Network, Tohoku University, Sendai, Miyagi 980-8577, Japan*
[6]*RIKEN Center for Emergent Matter Science, Wako 351-0198, Japan*

We develop a formulation of the coherent potential approximation (CPA) on the basis of the Wannier representation to advance a computationally efficient method for the treatment of homogeneous random alloys that is independent of the applied first-principles electronic structure code. To verify the performance of this CPA implementation within the Wannier representation, we examine the Bloch spectral function, the density of states, and the magnetic moment in Fe-based transition metal alloys Fe-X ($X = $ V, Co, Ni, and Cu) and compare the results with those of the well-established CPA implementation based on the Korringa-Kohn-Rostoker (KKR) Green's function method. The Wannier-CPA and the KKR-CPA methods lead to very similar results. The presented Wannier-CPA method has a wide potential applicability to other physical quantities and large compound systems because of the low computational effort required.

I. INTRODUCTION

Many substitutional alloys show a fascinating richness in their physical properties depending on their composition. For example, in spintronics, the spin Hall angle can be tuned by alloying [1]. Another example is the possibility to induce magnetism in semiconductors by the addition of impurities [2].

The methods to calculate the electronic structure of substitutional alloy systems have been developed since the 1930s [3–5]. The simplest approach for calculations for alloys is the virtual crystal approximation (VCA), in which the concentration average of the potential is placed on each site of the lattice [6,7]. Although the VCA seems to be a good approximation for metals with a simple free-electron-like electronic structure such as Na, K, and Al, it is known that the VCA completely fails to yield correct physical properties for transition metal alloys [4]. In particular, the VCA fails to describe element-specific properties of an alloy, which are relevant, for example, in hyperfine interactions [3]. This shortcoming of the VCA was removed by Korringa [8] and Beeby [9], who introduced the so-called average t-matrix approximation (ATA). Within this approach, the concentration average of the single-site scattering matrix, the t matrix, is used instead of the potential to consider component-projected properties. However, the ATA still has formal problems, sometimes leading to unphysical results [3]. For homogeneous random alloys, the

most sophisticated single-site method solving these problems is the coherent potential approximation (CPA). The CPA is a mean-filed theory treating alloys by introducing an effective medium defined by its average scattering properties first proposed by Soven [10] and Taylor [11]. Formulating the CPA within the framework of multiple scattering or Korringa-Kohn-Rostoker (KKR) formalism implies that embedding one of the alloy components in the CPA should lead to no additional scattering on average. Accordingly, unlike for the VCA and ATA methods, one has to determine the effective medium self-consistently for the CPA calculations.

As the CPA can easily be applied on the basis of electronic structure methods working with the Green's function, it is usually formulated in combination with the tight-binding (TB) method or the KKR Green's function method [12,13], which is a well-established first-principles electronic structure calculation method. Especially, using the KKR-CPA method [14,15], quite a few physical properties of alloy systems have been studied, such as the magnetic structure properties of dilute magnetic semiconductors [16], exchange coupling, and the corresponding magnetic transition temperature [17,18], as well as transport properties, such as the extrinsic and intrinsic contributions of the anomalous [19] and spin Hall effects [20]. This situation is due to a characteristic feature of the KKR method. Unlike other general first-principles calculation methods, such as the standard pseudopotential-based methods and the linearized augmented plane wave method, the Green's function of the system is used already within the self-consistent field (SCF) calculation step when performing KKR calculations. Therefore, it is easy to construct the Green's

[*]nao.ito@cmpt.phys.tohoku.ac.jp

function for alloy systems by means of the KKR-CPA and to directly calculate physical quantities using the resulting Green's function. In the field of first-principles calculations, the CPA is alternatively formulated on the basis of the tight-binding linear muffin-tin orbital method [21] as well as the linear combination of atomic orbitals methods [22,23].

In this contribution, we present an implementation of the CPA that is similar to the KKR-CPA Green's function method but more efficient and widely applicable while keeping the accuracy of the prediction of physical properties that the KKR-CPA method possesses. For the practical realization of this goal, we focus on the Wannier formulation. The reason for this is that we can construct Wannier functions from any kind of first-principles calculation method if the wave function is available, and we can set up a corresponding TB model from the obtained Wannier functions. This means that we present a computational method for the electronic structure of random alloys that can be combined with any kind of first-principles computational method. Moreover, we can substantially reduce the computational time when using the Wannier formalism if it is successfully combined with the CPA as it can be performed independently of the SCF calculations done by the first-principles calculations. However, the CPA method cannot be simply incorporated into the Wannier representation since two ambiguities remain in the calculation that do not exist in the KKR-CPA method. One is an ambiguity in the determination of the relative reference values of the on-site potentials for the elements that form an alloy since the SCF loops are executed independently for each element in the case of the Wannier representation. Concerning this problem, we propose a very simple method in Sec. II B to set the reference values from the results of some few supercell calculations. The other is setting the site off-diagonal terms for the CPA Hamiltonian. For the site off-diagonal terms, we employ the concentration average for each component of an alloy as it was applied in previous works dealing with the implementation of the CPA [13,22]. To clarify the validity of these two assumptions, it is quite important to compare basic physical quantities obtained with the Wannier-CPA method with those calculated using well-established CPA implementations such as the KKR-CPA method. Although works on alloys using the Wannier representation in combination with the CPA [24–33], the CPA+dynamical mean-field theory [34–36], the cluster coherent potential approximation [37,38], and the typical medium dynamical cluster approach [39] exist, there is no study testing the validity of the Wannier-CPA method by comparing physical quantities such as the spectral functions and the magnetic moments calculated by the Wannier-CPA method with those obtained for well-established and well-tested CPA implementations. Therefore, in this study, we test the performance of the Wannier-CPA method under these two assumptions and compare our results with the results from the KKR-CPA method. We will discuss the effect of the reference on-site potential in Sec. III C. Since the Wannier functions are widely used to investigate many physical properties [40,41], we can expect a wide range of applications of this method once the performance of the Wannier-CPA method becomes clear.

In the following, we first present our formulation of the CPA in terms of the Wannier representation. As examples

for its application, we show results for the Bloch spectral function, the density of states (DOS), and the magnetic moment in the Fe-based $3d$ transition metal alloys Fe-V, Fe-Co, Fe-Ni, and Fe-Cu. We verify the accuracy of the Wannier-CPA method by comparing the results with those calculated via the KKR-CPA method. Despite the rather simple formulation for the Wannier-CPA method, the quantities obtained in this way reproduce quite well the results obtained with the more demanding KKR-CPA method.

II. FORMULATION

To develop a simple and general computational method for homogeneous random alloys, we formulate the CPA on the basis of the Wannier formalism. We evaluate the performance of the Wannier-CPA method by comparing it with results obtained via the well-developed KKR-CPA calculation method. We first present the formulation of the CPA in random alloys as used within the KKR-CPA method and then adapt it for the Wannier representation.

A. KKR-CPA

The most prominent feature of the KKR Green's function method is that the Green's function of the system is set up and used during the SCF calculations. Within the KKR formalism, the Green's function for a pure system is given as follows [42]:

$$
\begin{aligned}
G(\boldsymbol{r} &+ \boldsymbol{R}_I + \boldsymbol{Q}_i, \boldsymbol{r}' + \boldsymbol{R}_J + \boldsymbol{Q}_j, E) \\
&= \sum_{\Lambda, \Lambda'} Z_\Lambda^i(\boldsymbol{r}, E) \tau_{\Lambda \Lambda'}^{IiJj}(E) Z_{\Lambda'}^{j \times}(\boldsymbol{r}', E) \\
&\quad - \delta_{IJ} \delta_{ij} \sum_\Lambda \left[Z_\Lambda^i(\boldsymbol{r}, E) J_\Lambda^{i \times}(\boldsymbol{r}', E) \theta(r' - r) \right. \\
&\quad \left. + J_\Lambda^i(\boldsymbol{r}, E) Z_\Lambda^{i \times}(\boldsymbol{r}', E) \theta(r - r') \right].
\end{aligned}
\tag{1}
$$

Here, $\boldsymbol{R}_I$ and $\boldsymbol{Q}_i$ give the positions of the unit cell I and atomic site i, respectively, and $\boldsymbol{r}$ and $\boldsymbol{r}'$ refer to the positions of electrons on atoms at $(\boldsymbol{R}_I, \boldsymbol{Q}_i)$ and $(\boldsymbol{R}_J, \boldsymbol{Q}_j)$, respectively. The functions Z_Λ^i and J_Λ^i stand for the regular and irregular solutions of the single-site Schrödinger or Dirac equation for site i, respectively. In the relativistic formulation, the subscript $\Lambda = (\kappa, \mu)$ stands for the combination of the relativistic spin-orbit (κ) and magnetic (μ) quantum numbers, and the superscript $\times$ refers to the left-hand-side solution of the Dirac equation [43]. The general definition of the scattering path operator $\tau_{\Lambda \Lambda'}^{IiJj}(E)$ accounts for all scattering events connecting site i of the Ith unit cell and site j of the Jth unit cell.

Since the Green's function of the system is obtained directly when using the KKR method, it is easy to calculate physical quantities or to incorporate the effect of alloying through the CPA; they can be formulated in terms of the Green's function. The CPA condition of the KKR formalism is formulated by the following equations [14]:

$$
\underline{\tau}_c^{0i0i}(E) = \sum_\alpha c_\alpha \underline{\tau}_\alpha^{0i0i}(E),
\tag{2}
$$

$$
\underline{\tau}_c^{0i0i}(E) = \frac{1}{\Omega_{\mathrm{BZ}}} \int_{\mathrm{BZ}} d^3 k \left[\underline{t}_c^{-1}(E) - \underline{\mathcal{G}}_0(\boldsymbol{k}, E) \right]_{ii}^{-1},
\tag{3}
$$

$$
\underline{\tau}_\alpha^{0i0i}(E) = \left[\underline{t}_\alpha^{i \, -1}(E) - \underline{t}_c^{i \, -1}(E) + \underline{\tau}_c^{0i0i \, -1}(E) \right]^{-1},
\tag{4}
$$

where $\underline{\tau}_c^{0i0i}(E)$ is the site-diagonal CPA scattering operator, the subscript α is the index for the atom types in the alloy, c_α is the concentration of atom α, Ω_{BZ} is the volume of the Brillouin zone (BZ), the underline indicates matrices on the basis of the combined spin angular momentum index Λ, and the double underline represents matrices with respect to the combined spin angular momentum index Λ and the site index i. The information about the coherent potential in a random alloy is included in $\underline{t}_c^i(E)$, which is the single-site scattering matrix for the coherent potential. The CPA scattering path operator $\underline{\tau}_c^{0i0i}(E)$ is given by the BZ integral in terms of the CPA single-site scattering matrix and so-called KKR structure constant $\underline{\mathcal{G}}_0(\boldsymbol{k}, E)$. The last equation gives the scattering path operator for an embedded α atom on site i in the CPA medium.

Unlike the previously mentioned VCA and ATA methods, we have to determine the CPA medium self-consistently for the given t matrices $\underline{t}_\alpha^i(E)$ of the components. Several algorithms have been suggested to deal with the above CPA equations. The most commonly used algorithm was worked out by Mills *et al.* [44] and allows one to obtain the CPA scattering path operator $\underline{\tau}_c^{0i0i}(E)$ using an iterative process (for more details, see Ref. [45]).

B. Wannier-CPA

While the Green's function is directly supplied by the KKR-CPA method, we first have to construct a TB Hamiltonian in the case of the Wannier formalism according to the expression

$$\mathcal{H} = \sum_{I,J} \sum_{i,j} \sum_{n,n'} |\boldsymbol{R}_I + \boldsymbol{Q}_i, n\rangle H_{nn'}^{IiJj} \langle \boldsymbol{R}_J + \boldsymbol{Q}_j, n'|, \quad (5)$$

where n is the index of the Wannier functions including spin. To make use of the CPA, we divide the Hamiltonian into site diagonal and off-diagonal terms as in the CPA, in which a single-site theory is formulated only for diagonal terms:

$$H_{nn'}^{IiJj} = (1 - \delta_{IJ}\delta_{ij})t_{nn'}^{IiJj} + \delta_{IJ}\delta_{ij}v_{nn'}^i, \quad (6)$$

where v and t are the on-site potential and the site off-diagonal terms of the Hamiltonian of the Wannier basis, respectively. To apply the CPA to the Wannier functions, we construct the Green's function of the system from the TB Hamiltonian. Within the Wannier representation, the corresponding real-space Green's function is given by an integral over the BZ as follows:

$$G_{nn'}^{0iJj}(E) = \frac{1}{\Omega_{BZ}} \int_{BZ} d^3k\, \mathcal{G}_{nn'}^{ij}(\boldsymbol{k}, E) e^{-i\boldsymbol{k}\cdot\boldsymbol{R}_J}, \quad (7)$$

where $\mathcal{G}_{nn'}^{ij}(\boldsymbol{k}, E)$ is the Fourier transform of the Green's function. Here, the Fourier transform reduces the computation time by reducing the number of matrix elements in the Green's function compared to the real-space representation. In matrix form, $\mathcal{G}_{nn'}^{ij}(\boldsymbol{k}, E)$ satisfies the following equation:

$$\underline{\underline{\mathcal{G}}}(\boldsymbol{k}, E) = \left[\underline{\underline{\mathcal{G}}}_0^{-1}(E) - \underline{\underline{\mathcal{T}}}(\boldsymbol{k})\right]^{-1}, \quad (8)$$

where matrices with both atomic site and Wannier function indices are indicated by a double underline. Here, the matrix elements are given by

$$[\underline{\underline{\mathcal{G}}}(\boldsymbol{k}, E)]_{nn'}^{ij} = \mathcal{G}_{nn'}^{ij}(\boldsymbol{k}, E), \quad (9)$$

$$[\underline{\underline{\mathcal{G}}}_0^{-1}(E)]_{nn'}^{ij} = \delta_{ij}(\delta_{nn'}E - v_{nn'}^i), \quad (10)$$

$$[\underline{\underline{\mathcal{T}}}(\boldsymbol{k})]_{nn'}^{ij} = \sum_J (1 - \delta_{0J}\delta_{ij})t_{nn'}^{0iJj} e^{i\boldsymbol{k}\cdot\boldsymbol{R}_J}. \quad (11)$$

The KKR multiple-scattering formulation for the CPA condition cannot be used within the Wannier formalism because of the complexity in defining the scattering path operator in the TB model. Therefore, we used an equation mathematically equivalent to the first equation in the KKR-CPA condition [see Eq. (2)]. For this purpose, we exploit the representation of the scattering operator $\underline{t}_\alpha^i(E)$,

$$\underline{t}_\alpha^i(E) = \left[\underline{v}_\alpha^i - \underline{v}_c^i(E)\right]\left\{1 - \underline{G}_c^{0i0i}(E)\left[\underline{v}_\alpha^i - \underline{v}_c^i(E)\right]\right\}^{-1}, \quad (12)$$

in which the fictitious coherent potential $\underline{v}_c^i(E)$ is replaced by the real potential of the α atom $\underline{v}_\alpha^i$ at site i. Herein, $\underline{G}_c^{0i0i}(E)$ corresponds to the Green's function of the coherent potential in the reference unit cell. The CPA condition in the single-site approximation is then given by

$$\langle \underline{t}^i \rangle = \sum_\alpha c_\alpha \underline{t}_\alpha^i = 0, \quad (13)$$

where we indicate the matrices with respect to the combined indices of the Wannier functions n by a single underline. For the numerical calculation of the coherent potential $\underline{v}_c^i(E)$, we use an iterative method that is similar to the Mills algorithm [46]. We update the nth temporary coherent potential $\underline{v}_c^{i\,(n)}(E)$ in the following way. When the CPA condition is not satisfied by the nth temporary coherent potential, we can define the concentration averaged scattering operator as

$$\langle \underline{t}^i \rangle^{(n)} = \sum_\alpha c_\alpha \underline{t}_\alpha^{i\,(n)} \neq 0. \quad (14)$$

The next update for the coherent potential is obtained as follows:

$$\underline{v}_c^{i\,(n+1)}(E) = \underline{v}_c^{i\,(n)}(E) + \langle \underline{t}^i \rangle^{(n)} \left[1 + \underline{G}_c^{0i0i(n)}(E)\langle \underline{t}^i \rangle^{(n)}\right]^{-1}, \quad (15)$$

where the Green's function is obtained from the nth coherent potential $\underline{v}_c^{i\,(n)}(E)$. We repeat the cycle until $\langle t_i \rangle^{(n)}$ becomes smaller than a threshold δ. We exploit the VCA for the initial guess of the coherent potential as follows:

$$\underline{v}_c^{i\,(1)}(E) = \sum_\alpha c_\alpha \underline{v}_\alpha^i. \quad (16)$$

To apply this formalism to real alloys, we have to consider the following two points. One is the on-site potentials of the two pure components since the density functional theory (DFT)-based Wannier Hamiltonian does not provide information about the reference value of these potentials. To determine the relative on-site potential energies, we use the supercell calculations as follows. Let us consider an *A*-*B* binary alloy. First, we perform DFT calculations for a supercell

of eight atoms, A_1B_7 and A_7B_1, and construct the TB Hamiltonian in the Wannier basis. Then, we derive the difference of the on-site potential of the $3d$ orbitals between components A and B for both A_1B_7 and A_7B_1 and set their average as $\Delta v_{A-B}^{\text{supercell}}$. Then, we perform DFT calculations for pure A and pure B and construct the Wannier TB Hamiltonian. We use this Hamiltonian to calculate the CPA Green's function, but before starting the CPA calculation, we subtract a constant from the diagonal terms of the on-site potential so that the potential difference of $3d$ orbitals in pure A and pure B becomes $\Delta v_{A-B}^{\text{supercell}}$. The other point to consider is the determination of the site off-diagonal term in the TB Hamiltonian since the site diagonal terms as well as the site off-diagonal terms are different for the two components. This is in sharp contrast to the KKR-CPA formalism, where only the scattering path operator depends on the component. In this paper, since we consider alloys consisting of two transition metal elements, we simply take a concentration average [13,22].

Accurate determination of the Fermi energy is important for examining the magnetic properties of alloys. We set the Fermi energy so that the total number of electrons

$$N = -\frac{1}{\pi} \text{Im Tr} \int^{E_F} dE \, \underline{\underline{G}}_c(E) \qquad (17)$$

is consistent with the number of electrons in the A-B alloy. A complex contour Gauss-Legendre integral is used to calculate the above integral. The Fermi energy of the system is determined iteratively using the DOS and the difference between the total number of electrons of the alloy and the number of electrons obtained by integrating the Green's function up to the temporary Fermi energy.

C. Computational steps of a Wannier-CPA calculation

The CPA calculations using the Wannier formalism are organized as follows: First, we perform DFT calculations using the QUANTUM ESPRESSO package [47,48] based on plane waves and pseudopotentials. We use the ultrasoft pseudopotentials [49] in the PSLIBRARY [50] with the functional type of a generalized gradient approximation with the Perdew-Burke-Ernzerhof exchange-correlation functional [51] and with relativistic effects included. Here, we set the lattice constant as the experimental value of bcc Fe $a = 2.86$ Å assuming that bcc Fe is alloyed with other transition metal elements.

The Wannierization process is conducted by using the WANNIER90 package [52–56] to reproduce the DFT energy bands below $E_F + 3$ eV, with E_F being the Fermi energy. We construct for each spin a nine-orbital model, which contains one $4s$, five $3d$, and three $4p$ atomic orbitals. Although we perform the Wannierization using wave functions obtained with the pseudopotential method, the underlying electronic structure calculation method used is irrelevant for the following discussion on the physical quantities. This implies in particular that our Wannier-CPA scheme can be combined with any band structure scheme that provides the corresponding Wannier representation of the electronic structure as an input.

Since the relative values of the reference for the on-site potential are not given by the Wannier Hamiltonian, we determine the difference of the on-site potential of $3d$ orbitals

between the Fe and X ($X = $ V, Co, Ni, and Cu) components by using $\Delta v_{\text{Fe}-X}^{\text{supercell}}$ calculated in the nonmagnetic mode. Using the on-site potential, we perform the Wannier-CPA calculations. We will discuss the dependence of the results on the constant subtracted from the on-site potential of X in the magnetic moment in the last part of Sec. III C.

The electronic structure calculation of the KKR-CPA method is performed self-consistently using the fully relativistic spin-polarized Munich SPR-KKR package [43,57]. For the exchange-correlation functional, we employ the parametrization given by Vosko *et al.* [58]. An angular momentum cutoff of $l_{\text{max}} = 4$ is used for the KKR multiple-scattering calculations. Here, we use the same lattice parameter $a = 2.86$ Å as in the Wannier-CPA calculation.

As the Green's function of a random alloy is obtained using the process described above, we can calculate the Bloch spectral function, the DOS, and the magnetic moment from the obtained CPA Green's function. In the following section, we describe the results of calculating these quantities in transition metal alloys and compare them with the results obtained with the KKR-CPA method.

III. RESULTS AND DISCUSSION

In this section, we present results for various physical quantities obtained using the Wannier-CPA method. We discuss their accuracy by comparing the Bloch spectral function, the DOS, and the magnetic moment calculated with the Wannier-CPA and the KKR-CPA methods. As an interesting target material, we focus on the Fe-based $3d$ transition metal alloys Fe-X ($X = $ V, Co, Ni, and Cu). We selected the elements X so that the atomic number of X is close to that of Fe. Here, we omit Fe-Cr and Fe-Mn alloys, for which an antiferromagnetic configuration is predicted in the alloy systems [59,60]. As is demonstrated in the following, we found excellent agreement between the results obtained with the Wannier-CPA and KKR-CPA methods for the considered alloys.

A. Bloch spectral function

First, we show the Bloch spectral functions of bcc Fe-Cu alloys calculated using both the Wannier-CPA and KKR-CPA methods to compare the basic electronic structure that determines physical quantities. The Bloch spectral function is the imaginary part of the trace of the Green's function given as follows:

$$A(\boldsymbol{k}, E) = -\frac{1}{\pi} \text{Im Tr} \, \underline{\underline{\mathcal{G}}}_c(\boldsymbol{k}, E). \qquad (18)$$

If we plot the wave vector and energy region where the Bloch spectral function takes finite values, it shows a structure very similar to the band structure or dispersion relation $E(\boldsymbol{k})$ of the pure systems. Figure 1 shows the representative Bloch spectral function for bcc Fe$_x$Cu$_{1-x}$ ($x = 0.0, 0.2, 0.4, 0.6, 0.8$, and 1.0) alloys calculated using both the Wannier-CPA (left side) and the KKR-CPA (right side) methods. We obtained similar behavior for the Bloch spectral function of Fe-V, Fe-Co, and Fe-Ni alloys. For this reason, we discuss only the details of the calculations of the bcc Fe-Cu alloys. The calculations were performed using the bcc structure for all the calculations on Fe-Cu alloys for simplicity, although Cu takes the fcc structure
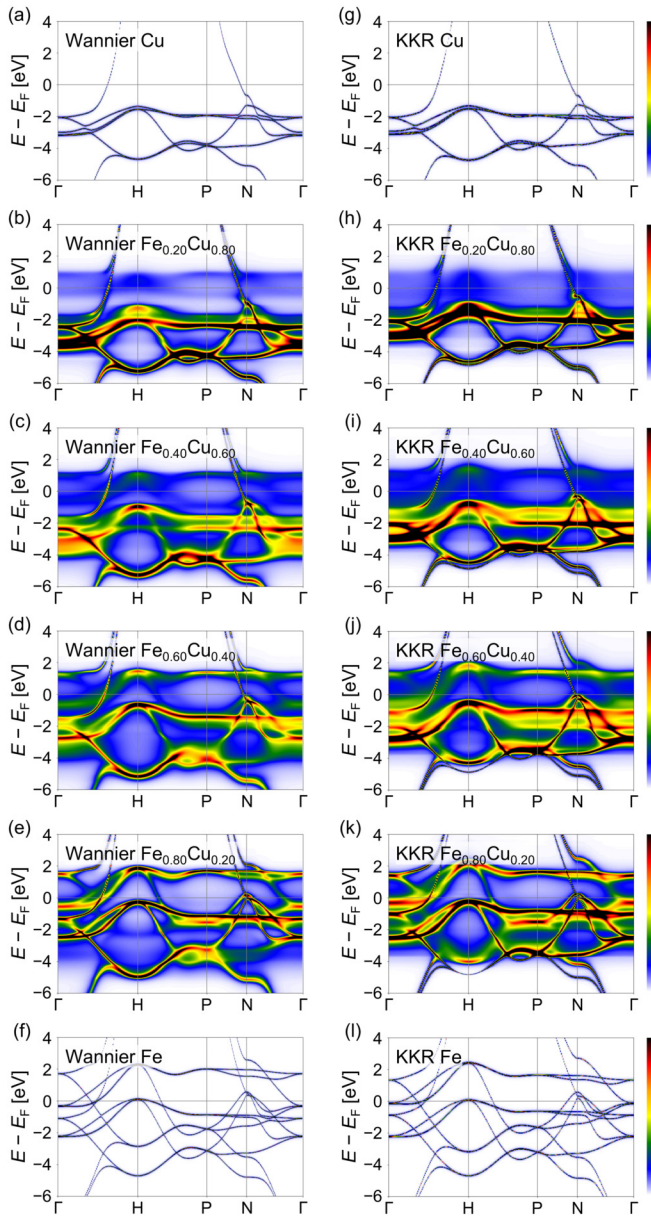
FIG. 1. Bloch spectral functions along the high-symmetry lines Γ-H-P-N-Γ for Fe_xCu_{1-x} with the concentrations (a) $x = 0.00$, (b) $x = 0.20$, (c) $x = 0.40$, (d) $x = 0.60$, (e) $x = 0.80$, and (f) $x = 1.00$ calculated by the Wannier-CPA method and (g) $x = 0.00$, (h) $x = 0.20$, (i) $x = 0.40$, (j) $x = 0.60$, (k) $x = 0.80$, and (l) $x = 1.00$ calculated by the KKR-CPA method.

FIG. 2. The same as Fig. 1, but projected to spin-down states.

in the pure form. Similarly, the calculations for the Fe-V, Fe-Co, and Fe-Ni alloys were also performed by using the bcc structure. For the calculation for pure Fe and Cu, we added a small imaginary part of 0.1 mRy to the energy to obtain visible Bloch spectra because the spectral structure consists of a δ function for pure Fe and Cu. As shown in Fig. 1, we obtain very close spectral structures from the Wannier-CPA and KKR-CPA methods.

Since the Bloch spectral functions of the total state have a rather complex structure, we resolved them with respect to the spin directions. The corresponding Bloch spectral functions for the spin-down and -up states in Fe_xCu_{1-x} are represented

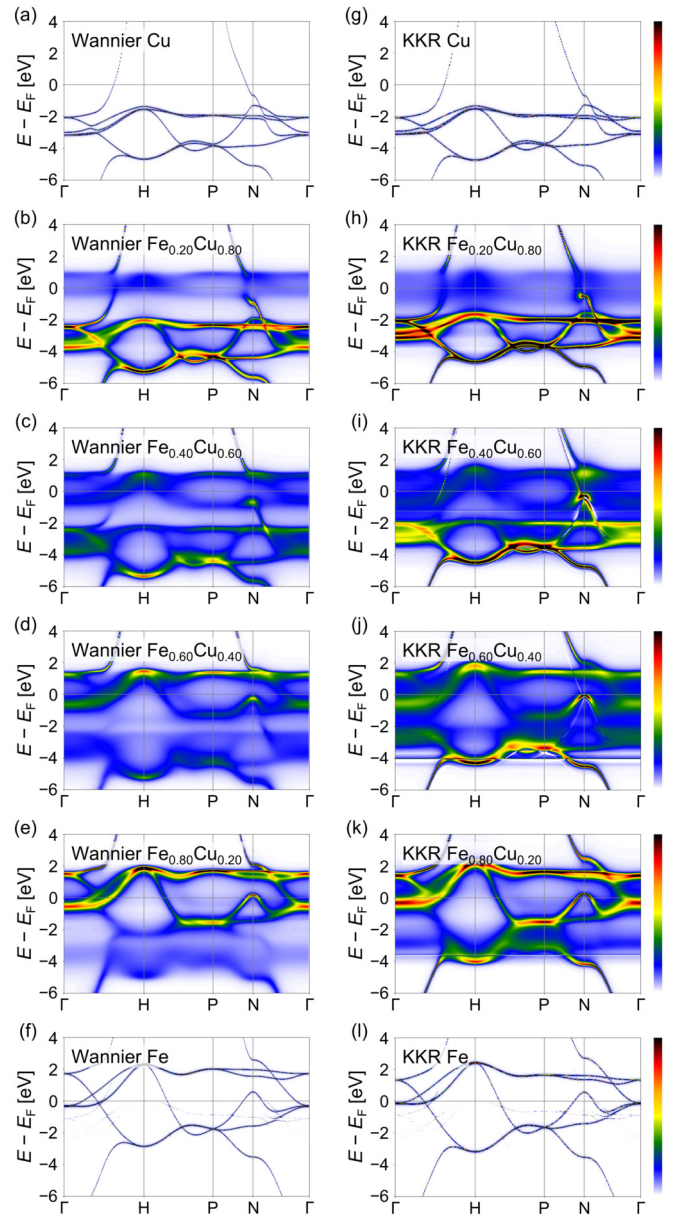in Figs. 2 and 3, respectively. As the concentration is changed from Cu to $Fe_{0.20}Cu_{0.80}$, the spectral structure of Fe appears between -1 and 1 eV in both the Wannier-CPA and the KKR-CPA results, as shown in Figs. 2(b) and 2(h), which is about 2 eV lower than that for pure Fe. This spectral structure becomes clear and shifts to higher energies as the concentration of Fe is increased to 0.40 and 0.60 in both methods.

The only major difference in the Bloch spectral function between the Wannier-CPA and the KKR-CPA results appears in the spectral structure of $Fe_{0.80}Cu_{0.20}$ near the H point in the reciprocal lattice. We observed a pronounced structure near -2 eV in the case of the Wannier-CPA method, as shown in Fig. 2(e), which is strongly affected by the spectral structure of Fe. On the other hand, in the KKR-CPA method, this feature is mixed with the spectrum of Cu at around -5 eV, forming a single-peak structure [Fig. 2(k)].
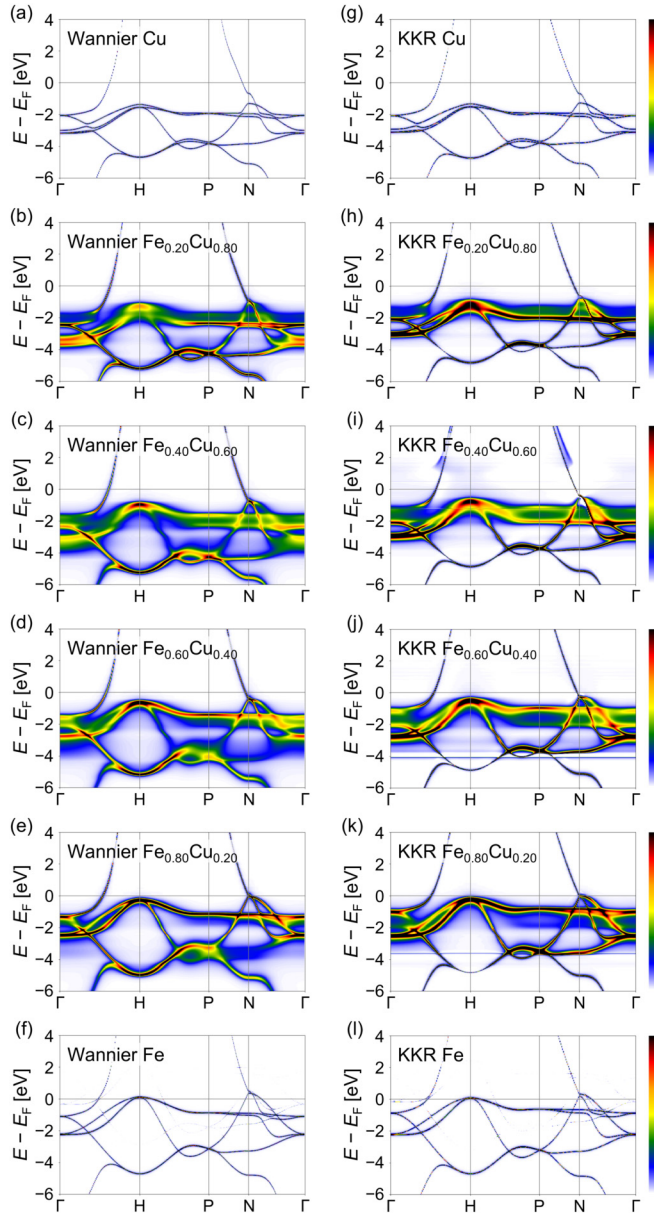
FIG. 3. The same as Fig. 1, but projected to spin-up states.

FIG. 4. DOS of Fe$_x$X$_{1-x}$, where X atoms are (a) V, (b) Co, (c) Ni, and (d) Cu alloys calculated by the Wannier-CPA method and (e) V, (f) Co, (g) Ni, and (h) Cu alloys calculated by the KKR-CPA method. The DOS of pure Fe is shown by red lines, and that of X is shown by blue lines. For alloys, we show the DOS using intermediate colors between red and blue depending on the concentrations of Fe and X.

For pure bcc Fe, we observed weak spectral features in the spin-down channel that reflect the main spectra of the spin-up states between -2 and 2 eV in the results obtained with the Wannier-CPA and the KKR-CPA methods [Figs. 2(f) and 2(l)]. These weak features can be ascribed to the relativistic effect of the mixing of spin-up and spin-down states by the spin-orbit coupling.

Figure 3 shows the Bloch spectral functions for the spin-up states in Fe$_x$Cu$_{1-x}$ calculated using both the Wannier-CPA and KKR-CPA methods. Unlike the spectral structure of Fe$_{0.20}$Cu$_{0.80}$ in the spin-down state, the blurred spectral structure near the Fermi energy does not show up in the spin-up state, as shown in Figs. 3(b) and 3(h), forming a sharper structure over the entire region. This so-called virtual-crystal-like behavior indicates that the spin-up spectra of pure Fe and Cu are energetically closer to each other than those of the
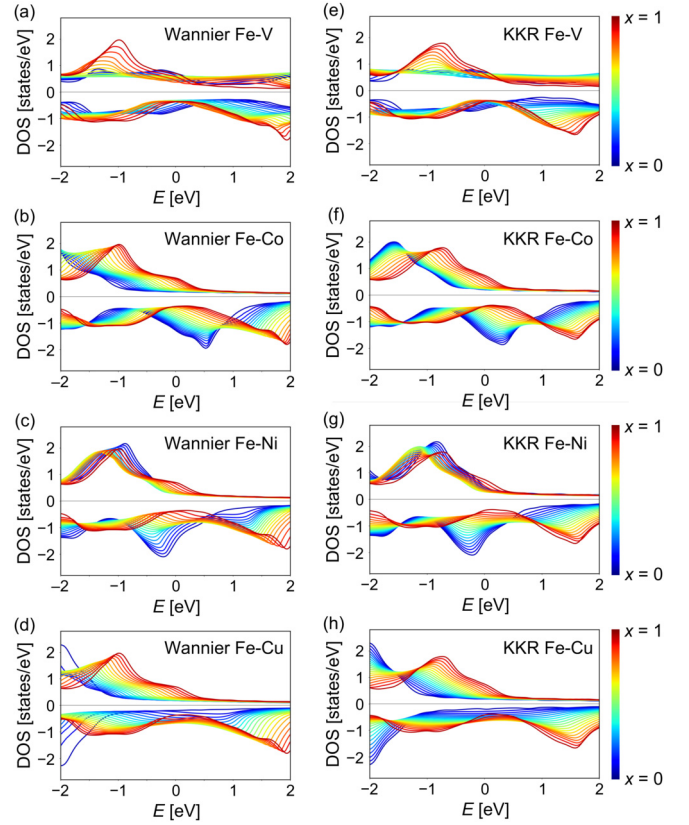
spin-down states. For the same reason, the spectral structures between -6 and -4 eV are less blurred than those between -3 and -1 eV in Fe$_x$Cu$_{1-x}$ ($x = 0.20$–0.80) alloys since the spectral structure of pure Fe and Cr are energetically closer to each other between -6 and -4 eV. This behavior was observed for both the Wannier-CPA and KKR-CPA methods [Figs. 3(b)–3(e) and 3(h)–3(k)]. We again observed a weak spectral feature corresponding to the main spectral structure of the spin-down states in pure Fe between energies of -2 and 1 eV [Figs. 3(f) and 3(l)].

B. Density of states

Figure 4 shows the computational results for the DOS near the Fermi energy (-2 to 2 eV) obtained with the Wannier-CPA and KKR-CPA methods for bcc Fe-X ($X =$ V, Co, Ni, and Cu) alloys to monitor the occupation trend of the states in each alloy. Here, the DOS is given by integrating the Bloch spectral functions over the BZ:

$$D(E) = \int_{BZ} d^3k \, A(\boldsymbol{k}, E). \tag{19}$$

We plot the DOS of pure Fe and the pure X component with red and blue lines, respectively. For the alloy systems, we plot the DOS with a neutral color between red and blue depending
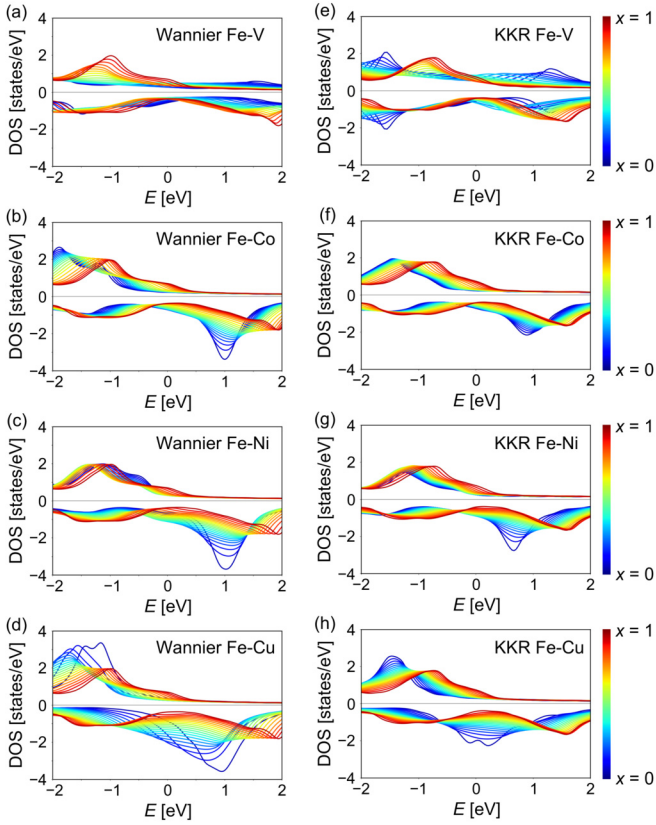
FIG. 5. The same as Fig. 4, but projected to the Fe component.

FIG. 6. The same as Fig. 4, but projected to the X component (X = V, Co, Ni, and Cu).

on the concentrations of Fe and X. Figure 4 shows that the qualitative behavior of the DOS energy shift with increasing X concentration is fully consistent for both the Wannier-CPA and KKR-CPA methods. A representative example can be seen in the spin-up DOS of Fe-Ni alloys. For the KKR-CPA method [Fig. 4(g)], the peak structure arising from Fe at around -1 eV is shifted to lower energies as the concentration of Ni increases, reaching a minimum at around $Fe_{0.50}Ni_{0.50}$, and is then shifted to higher energies. This behavior is reproduced quite well by the Wannier-CPA calculations, as shown in Fig. 4(c).
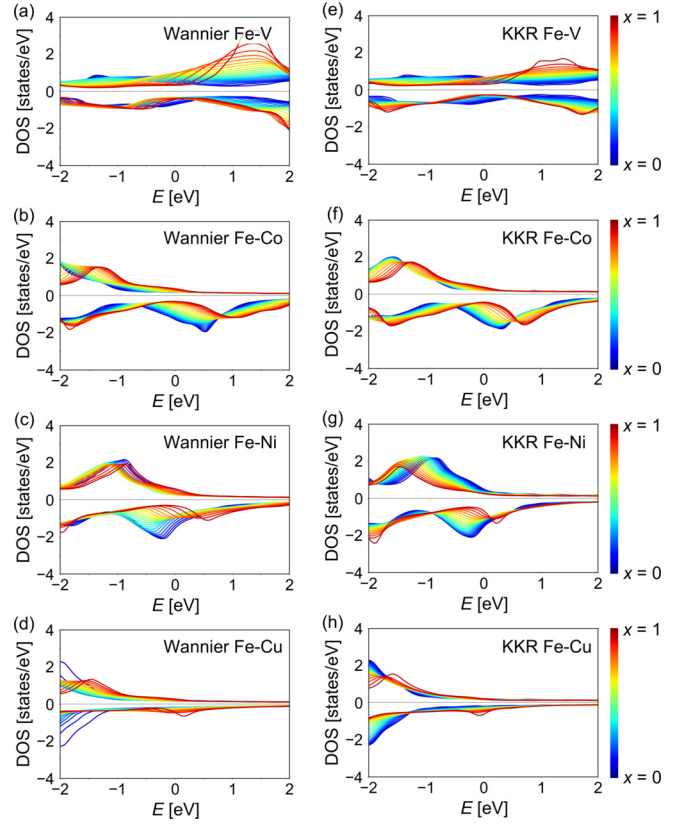
To examine the element-specific properties of the DOS, we define the component projection of the Green's function. According to Ref. [14], the CPA condition given by Eq. (13) can be rewritten using the Green's function as follows:

$$\underline{G}_c^{0i0i}(E) = \sum_\alpha c_\alpha \underline{G}_\alpha^{0i0i}(E), \qquad (20)$$

where $\underline{G}_\alpha^{0i0i}(E)$ is given by

$$\underline{G}_\alpha^{0i0i}(E) = \underline{G}_c^{0i0i}(E) + \underline{G}_c^{0i0i}(E)\underline{t}_\alpha^i(E)\underline{G}_c^{0i0i}(E). \qquad (21)$$

Here, $\underline{G}_\alpha^{0i0i}(E)$ gives the Green's function when, for site i of the zeroth unit cell, the t matrix of the CPA medium is replaced by that for component α. Therefore, $\underline{G}_\alpha^{0i0i}(E)$ corresponds to the α-component projection of the CPA Green's function. As the component projection of the Green's function is determined in the CPA cycle, the calculation of the element-specific properties of the DOS is straightforward. Figures 5 and 6 show the Fe- and X-specific DOSs of Fe-X (X = V,

Co, Ni, and Cu) alloys, respectively. Here, again, the DOS of the alloy with a high Fe concentration is plotted with reddish lines, and that with a high X concentration is shown by bluish lines. On the whole, structural similarities in the element-specific DOSs calculated with both the Wannier-CPA and KKR-CPA methods can be found in Figs. 5 and 6, but we can also see some small differences in the detailed structure.

For example, the Fe-component projection of the DOS of Fe-V alloys in the V-rich region obtained with the KKR-CPA method has a peak structure near -1.5 eV [Fig. 5(e)] which is not observed in the spin-up DOS and quite small in the spin-down DOS of the Wannier-CPA calculation [Fig. 5(a)].

C. Magnetic moment

In the previous two sections, we found that the Wannier-CPA method can reproduce the Bloch spectral function and the DOS of Fe-based transition metal alloys quite well. Finally, we discuss the physical quantities predicted by the Wannier-CPA method. As an example, we focus on the magnetic moment. Concerning the magnetic moment in Fe-based transition metal alloys, one of the best benchmarks is the Slater-Pauling curve [61]. The Slater-Pauling curve is a convex curve that appears when the saturation magnetization of these alloys is plotted against the number of electrons per atom. In Fe-Co alloys, it is known that the maximum of the saturation magnetization occurs near $Fe_{0.7}Co_{0.3}$. The left and right sides of the curve form a straight line with an angle of $45°$ with the horizontal axis of the Fe-based alloys when the
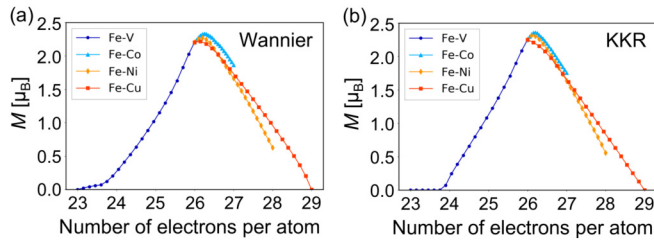
FIG. 7. Magnetic moment of Fe-X (X = V, Co, Ni, and Cu) calculated by (a) the Wannier-CPA and (b) KKR-CPA methods.

scales of one electron on the horizontal axis and one Bohr magneton on the vertical axis are equal. Previous research showed that the experimental results of the Slater-Pauling curve are excellently reproduced by the KKR-CPA calculations [62,63]. Here, we compare our results for the magnetic moment obtained with our Wannier-CPA method with those of the KKR-CPA method.

Figure 7 shows the magnetic moment in the Fe-X (X = V, Co, Ni, and Cu) alloys calculated by the Wannier-CPA and KKR-CPA methods. There is a structural transition from bcc to fcc in Fe-based alloys when the number of electrons exceeds about 26.7. However, all the calculations were done in the bcc structure for the one-to-one comparison between the Wannier-CPA and KKR-CPA methods. We can conclude from Fig. 7 that the Wannier-CPA calculation gives reliable calculation results concerning the calculation of magnetic moments for the following reasons. First of all, the magnetic moments calculated by the Wannier-CPA method form a typical Slater-Pauling curve, which takes a maximum moment in the case of $Fe_{0.75}Co_{0.25}$ and intersects the horizontal axis at an angle of almost $45°$. Furthermore, the calculated magnetic moments in the bcc Fe-X (X = V, Co, Ni, and Cu) alloys using the Wannier-CPA method are in good agreement with those from the KKR-CPA method since the average values of the deviation in magnetic moments are only $0.057\mu_B$, $0.064\mu_B$, $0.036\mu_B$, and $0.080\mu_B$, respectively. These results show that the Wannier-CPA method can be a powerful tool for the prediction of physical quantities expressed by the integral up to Fermi energy despite its simple formulation.

Since we set the reference values of the on-site potential using a simple method using supercell calculations, we discuss the effect of the change in the magnetic moment due to deviation from the actual reference values of the on-site potential. Since the difference in $\Delta v_{Fe-X}^{supercell}$ (X = V, Co, Ni, and Cu) obtained from Fe_1X_7 and Fe_7X_1 is within 1 eV [64], we calculated the magnetic moment of $Fe_{0.5}X_{0.5}$ by adding 0.5 eV to the diagonal terms of the on-site potential of X in the Wannier-CPA method. Then, we calculated the magnetic moment by subtracting 0.5 eV from the diagonal terms of the on-site potential of X and derived the difference between the two moments. We divided it by the magnetic moment calculated without changing the on-site potential and derived the rates of change in the magnetic moment. These rates of change in the magnetic moment were only 6.55%, 2.07%, 0.23%, and 4.72% in $Fe_{0.5}V_{0.5}$, $Fe_{0.5}Co_{0.5}$, $Fe_{0.5}Ni_{0.5}$, and $Fe_{0.5}Cu_{0.5}$, respectively, even with the large difference of 1 eV in the on-site potential. Since the difference in the reference

values of the on-site potentials between Fe and X from the actual values has only a small effect on the physical quantities, this method using supercells can be a simple and valuable way to determine the relative difference in the on-site potentials of Fe and X.

IV. CONCLUSION

We have formulated the CPA in the Wannier representation to develop a calculation method for homogeneous random alloys, which can be readily accessed from any first-principles calculation method. This Wannier-CPA method significantly reduces the computation time compared with those of the existing methods. Compared to the KKR-CPA method, this Wannier-CPA method can be expected to reduce the computational time by a factor of 10. To investigate the performance of this Wannier-CPA method, we have examined the Bloch spectral function, the DOS, and the magnetic moment for various Fe-based transition metal alloys from the Green's function obtained with the Wannier-CPA method and compared our results with the results of the calculation using the well-developed KKR-CPA method. Regarding the Bloch spectral function, the spectral structures of the Fe-Cu alloys were compared using both the Wannier-CPA and KKR-CPA methods. We observed a blurred spectral structure of Fe near the Fermi energy in the spin-down state when the Fe content was low. On the other hand, we observed a clear virtual-crystal-like spectral structure in the spin-up state. This is because of the similarity in the energy structures of Fe and Cu spin-up states. These behaviors are the same in both the Wannier-CPA and KKR-CPA methods. Furthermore, by changing the concentration of Fe, we also found an energy shift in the peak structure of the DOS. It is the same for the Wannier-CPA and KKR-CPA calculations for all of the Fe-X (X = V, Co, Ni, and Cu) alloys. Finally, we calculated the magnetic moment of the Fe-X alloys. We can reproduce the well-known Slater-Pauling curve from the Wannier-CPA method, which is quite similar to that from the KKR-CPA method, which confirms the good predictive power for physical quantities of the Wannier-CPA method. In this paper, we have discussed only the Bloch spectral function, the DOS, and the magnetic moment in the Wannier-CPA method. Nevertheless, one may conclude that this Wannier-CPA method has great applicability to other physical quantities and also large compound systems, which have many restrictions concerning the calculation time as the main bottleneck. The transport calculation should be one such example. Although there are many works on the anomalous and spin Hall effects using Wannier functions, only the intrinsic contribution of the conductivity is considered in all those works. Using the formulation we have given, it could be possible to calculate the conductivity including the extrinsic contributions as well. To evaluate the potential of the developed Wannier-CPA method, we expect further applications of the method to various materials in addition to transition metal alloys.

[1] M. Obstbaum, M. Decker, A. K. Greitner, M. Haertinger, T. N. G. Meier, M. Kronseder, K. Chadova, S. Wimmer, D. Ködderitzsch, H. Ebert, and C. H. Back, Phys. Rev. Lett. **117**, 167204 (2016).

[2] J. K. Furdyna, J. Appl. Phys. **64**, R29 (1988).

[3] J. S. Faulkner, Prog. Mater. Sci. **27**, 1 (1982).

[4] W. M. Temmerman and Z. Szotek, Comput. Phys. Rep. **5**, 173 (1987).

[5] E. N. Economou, *Green's Functions in Quantum Physics* (Springer, Berlin, 2006).

[6] L. Nordheim, Ann. Phys. (Berlin, Ger.) **401**, 607 (1931).

[7] T. Muto, Sci. Pap. Inst. Phys. Chem. Res. **34**, 377 (1938).

[8] J. Korringa, J. Phys. Chem. Solids **7**, 252 (1958).

[9] J. Beeby, Phys. Rev. **135**, A130 (1964).

[10] P. Soven, Phys. Rev. **156**, 809 (1967).

[11] D. W. Taylor, Phys. Rev. **156**, 1017 (1968).

[12] H. Shiba, Prog. Theor. Phys. **46**, 77 (1971).

[13] B. L. Gyorffy and G. M. Stocks, J. Phys. (Paris) **35**, C4–75 (1974).

[14] B. L. Gyorffy, Phys. Rev. B **5**, 2382 (1972).

[15] J. S. Faulkner and G. M. Stocks, Phys. Rev. B **21**, 3222 (1980).

[16] H. Akai, Phys. Rev. Lett. **81**, 3002 (1998).

[17] K. Sato, P. H. Dederichs, and H. Katayama-Yoshida, Hyperfine Interact. **160**, 57 (2005).

[18] H. Ebert and S. Mankovsky, Phys. Rev. B **79**, 045209 (2009).

[19] S. Lowitzer, D. Ködderitzsch, and H. Ebert, Phys. Rev. Lett. **105**, 266604 (2010).

[20] S. Lowitzer, M. Gradhand, D. Ködderitzsch, D. V. Fedorov, I. Mertig, and H. Ebert, Phys. Rev. Lett. **106**, 056601 (2011).

[21] J. Kudrnovský, V. Drchal, and J. Mašek, Phys. Rev. B **35**, 2487 (1987).

[22] R. Richter, H. Eschrig, and B. Velicky, J. Phys. F **17**, 351 (1987).

[23] R. Richter and H. Eschrig, J. Phys. F **18**, 1813 (1988).

[24] D. Mourada and G. Czycholl, Eur. Phys. J. B **85**, 153 (2012).

[25] M. A. Korotin, N. A. Skorikov, V. M. Zainullina, E. Z. Kurmaev, A. V. Lukoyanov, and V. I. Anisimov, JETP Lett. **94**, 806 (2011).

[26] M. A. Korotin, A. V. Efremov, E. Z. Kurmaev, and A. Moewes, JETP Lett. **95**, 641 (2012).

[27] V. M. Zainullina and M. A. Korotin, Phys. Solid State **55**, 26 (2013).

[28] M. A. Korotin and V. M. Zainullina, Phys. Solid State **55**, 952 (2013).

[29] M. A. Korotin, Z. V. Pchelkina, N. A. Skorikov, E. Z. Kurmaev, and V. I. Anisimov, J. Phys.: Condens. Matter **26**, 115501 (2014).

[30] M. A. Korotin, Z. V. Pchelkina, N. A. Skorikov, V. I. Anisimov, and A. O. Shorikov, J. Phys.: Condens. Matter **27**, 045502 (2015).

[31] M. A. Korotin, N. A. Skorikov, A. V. Efremov, and A. O. Shorikov, J. Magn. Magn. Mater. **397**, 115 (2016).

[32] M. A. Korotin, N. A. Skorikov, and A. O. Anokhin, Phys. B (Amsterdam, Neth.) **526**, 14 (2017).

[33] M. A. Korotin, Z. V. Pchelkina, N. A. Skorikov, A. V. Efremov, and V. I. Anisimov, Phys. Met. Metallogr. **117**, 655 (2016); V. M. Zainullina and M. A. Korotin, JETP Lett. **114**, 296 (2021).

[34] A. S. Belozerov, A. I. Poteryaev, S. L. Skornyakov, and V. I. Anisimov, J. Phys.: Condens. Matter **27**, 465601 (2015).

[35] A. I. Poteryaev, N. A. Skorikov, V. I. Anisimov, and M. A. Korotin, Phys. Rev. B **93**, 205135 (2016).

[36] A. S. Belozerov and V. I. Anisimov, J. Phys.: Condens. Matter **28**, 345601 (2016).

[37] M. Köhl, C. Wolff, and K. Busch, Opt. Lett. **37**, 560 (2012).

[38] M. Köhl, C. Wolff, and K. Busch, J. Opt. Soc. Am. B **31**, 2246 (2014).

[39] H. Terletska, Y. Zhang, K.-M. Tam, T. Berlijn, L. Chioncel, N. S. Vidhyadhiraja, and M. Jarrell, Appl. Sci. **8**, 2401 (2018).

[40] N. Marzari, A. A. Mostofi, J. R. Yates, I. Souza, and D. Vanderbilt, Rev. Mod. Phys. **84**, 1419 (2012).

[41] T. Nomoto, T. Koretsune, and R. Arita, Phys. Rev. B **102**, 014444 (2020).

[42] P. Weinberger, *Electron Scattering Theory for Ordered and Disordered Matter* (Oxford University Press, Oxford, 1990).

[43] H. Ebert, D. Ködderitzsch, and J. Minár, Rep. Prog. Phys. **74**, 096501 (2011).

[44] R. Mills, L. J. Gray, and T. Kaplan, Phys. Rev. B **27**, 3252 (1983).

[45] B. Ginatempo and J. B. Staunton, J. Phys. F **18**, 1827 (1988).

[46] M. Wołoszyn and A. Z. Maksymowicz, Task Q. **6**, 669 (2002).

[47] P. Giannozzi *et al.*, J. Phys.: Condens. Matter **21**, 395502 (2009).

[48] P. Giannozzi *et al.*, J. Phys.: Condens. Matter **29**, 465901 (2017).

[49] A. Dal Corso and A. Mosca Conte, Phys. Rev. B **71**, 115106 (2005).

[50] A. D. Corso, Comput. Mater. Sci. **95**, 337 (2014).

[51] J. P. Perdew, K. Burke, and M. Ernzerhof, Phys. Rev. Lett. **77**, 3865 (1996).

[52] N. Marzari and D. Vanderbilt, Phys. Rev. B **56**, 12847 (1997).

[53] I. Souza, N. Marzari, and D. Vanderbilt, Phys. Rev. B **65**, 035109 (2001).

[54] A. A. Mostofi, J. R. Yates, Y.-S. Lee, I. Souza, D. Vanderbilt, and N. Marzari, Comput. Phys. Commun. **178**, 685 (2008).

[55] A. A. Mostofi, J. R. Yates, G. Pizzi, Y.-S. Lee, I. Souza, D. Vanderbilt, and N. Marzari, Comput. Phys. Commun. **185**, 2309 (2014).

[56] G. Pizzi *et al.*, J. Phys.: Condens. Matter **32**, 165902 (2020).

[57] H. Ebert *et al.*, The Munich spin-polarized relativistic Korringa-Kohn-Rostoker (SPR-KKR) package, version 8.5.0, 2020, https://www.ebert.cup.uni-muenchen.de/index.php/en/software-en/13-sprkkr.

[58] S. H. Vosko, L. Wilk, and M. Nusair, Can. J. Phys. **58**, 1200 (1980).

[59] K. Hirai, J. Phys. Soc. Jpn. **67**, 1776 (1998).

[60] A. Sakuma, J. Phys. Soc. Jpn. **67**, 2815 (1998).

[61] R. M. Bozorth, *Ferromagnetism* (Van Nostrand, New York, 1951).

[62] P. H. Dederichs, R. Zeller, H. Akai, and H. Ebert, J. Magn. Magn. Mater. **100**, 241 (1991).

[63] H. Akai, Hyperfine Interact. **68**, 3 (1992).

[64] The average and the difference of $\Delta v_{\text{Fe}-X}^{\text{supercell}}$ obtained from $\text{Fe}_1 X_7$ and $\text{Fe}_7 X_1$ (X = V, Co, Ni, and Cu) are -1.75 and 0.824 eV for V, 0.803 and 0.0656 eV for Co, 0.885 and 0.0599 eV for Ni, and 2.28 and 0.530 eV for Cu.